PAPER

Check for updates

Activated carbon *versus* montmorillonite embedded on porous chitosan beads for the treatment of olive mill wastewater: a comparative study

Wahid Ben Khadda, [a] Oumaima Bahammou,[b] Farah El Hassani,[a] Nadia Katir,[a] Hicham Zaitan[b] and Abdelkrim El Kadib *[ac]

Efficient adsorbents require functional groups capable of strong coordination with surrounding species, combined with an open porous network that facilitates pollutant diffusion and storage. Conventional strategies to generate porosity typically rely on structure-directing agents, which are subsequently removed through time-consuming, energy-intensive, and environmentally unsustainable thermal or chemical treatments. Diverging from these traditional approaches, colloidal polysaccharides offer a sustainable alternative, forming inherently porous hydrogels that serve as self-supporting reactors for water purification. In this work, we harnessed this property to transform discarded seafood bio-waste chitosan into highly reactive adsorbents for the treatment of olive mill wastewater. To enhance polyphenol uptake, various exogenous nanoparticles were incorporated within the hydrogel matrix, among which activated carbon and, to a lesser extent, montmorillonite clay proved most effective. Adsorption tests were performed using syringic acid and caffeic acid as model polyphenols representative of olive mill effluents, followed by trials on real industrial wastewater. Unlike conventional powdered adsorbents, the self-standing nature and macroporous architecture of the chitosan beads offer significant advantages in terms of recyclability and handling. Furthermore, beads enriched with polyphenolic extracts can be repurposed for the subsequent removal of dyes, antibiotics, and copper contaminants.

Sustainability spotlight

While olive oil constitutes a vibrant economic sector for many countries (mainly Mediterranean countries), this activity is unfortunately also generating a huge amount of pollution, known as olive mill wastewater pollution, making its treatment a big challenge. While synthetic adsorbents could be an option for its removal, we present herein an approach based on the circular economy to transform discarded fishery waste into highly reactive adsorbents. We have used a natural polymer extracted from shellfish (chitosan) to craft highly porous hydrogels. The use of the latter as a carrier for active carbon allowed efficient removal of polyphenols and also an easy separation of the gels from the medium. The resulting polyphenol-enriched hydrogels can moreover be used to chelate other chemicals, which is very appealing for further utilisation.

Introduction

Olive oil extraction consumes water during various stages, including washing, cleaning, crushing, grinding, malaxation, and centrifugation, and inevitably generates a large volume of pollutants known as olive mill wastewater (OMW).[1–3] OMW consists of water contaminated with high loads of organic matter, suspended solids, polyphenols, sugars, and other substances, including toxic compounds.[4] Its composition varies depending on several factors such as olive variety, processing methods, and the equipment employed.[5] Consequently, it is crucial to establish straightforward and industrially scalable technologies for OMW management and treatment to minimize its environmental impact and ensure compliance with wastewater disposal regulations.[6]

Several methods are available for OMW treatment, including physical, chemical, and biological processes,[7] while their combined use is often adopted to enhance overall treatment efficiency.[8,9] Although advanced photo-oxidation pathways are highly effective for water purification, completely mineralizing organic pollutants into water and carbon dioxide, they do not align with circular economy principles, as they eliminate rather than valorise pollutants. In contrast, adsorption removes

[a]Euromed University of Fes, UEMF, Morocco. E-mail: a.elkadib@ueuromed.org

[b]Processes, Materials and Environment Laboratory (LPME), Faculty of Sciences and Technology of Fez, Sidi Mohamed Ben Abdellah University, B. P. 2202 Fez, Morocco

[c]Hassan II Academy of Science and Technology, Rabat, Morocco

contaminants from water without destroying them, thus enabling their recovery and potential reuse.[10] This makes the development of multifunctional adsorbents for OMW treatment an emerging research niche, where both process efficiency and carbon footprint are key considerations.[11] Accordingly, growing attention has been directed toward adsorbents derived from natural or waste-based sources, aiming to achieve closed-loop circularity and sustainable waste valorization.[12]

A notable example of "waste-to-wealth" transformation is the valorization of seafood by-products to extract chitin, a fully acetylated polysaccharide that ranks as the second most abundant biopolymer after cellulose, with an estimated annual production approaching ten gigatons.[13,14] Although chitin is insoluble and structurally recalcitrant, its deacetylation yields chitosan, a derivative with numerous advantageous properties, including high chemical reactivity, structural tunability, and textural moldability.[15,16] Designing functional nanomaterials from chitosan therefore aligns with the principles of the circular economy and addresses multiple challenges in sustainable development.[17]

In this context, we have previously engineered various chitosan-based microspheres,[18–20] with particular focus on their applications in dye and CO_2 adsorption,[21–23] as well as in metal-supported heterogeneous (photo)catalysis.[24–27] We successfully entrapped a range of nano-objects within chitosan matrices, including clay nanoparticulates,[21] graphene oxide sheets,[28] carbon nitride,[27] boron nitride,[29] and a mechanically ground titanium dioxide–graphene oxide mixture.[27] Remarkably, such entrapment did not compromise the microsphere shape, quality, homogeneity, network porosity, or accessibility of active sites. Furthermore, chitosan retained its gelling ability, allowing the formation of self-standing microspheres even at high filler loadings.[28,29]

Building upon our previous experience in fabricating chitosan-based microspheres,[30] we hypothesized that these porous structures could be adapted for OMW treatment. To this end, we investigated the incorporation of different reactive fillers during chitosan gelation, including nanosized clay and activated carbon, both known for their high adsorption capacity toward water pollutants.[31,32] Hitherto, conventional adsorbents have suffered from limited contaminant removal efficiency, lack of antibacterial activity, rapid saturation and clogging, and inability to soften water.[33–36] Moreover, their powdery nature poses handling challenges, requiring tedious recovery procedures and frequent replacement, with minimal recyclability.[37,38] The use of porous chitosan-based beads hosting reactive adsorbents thus offers a more practical solution, facilitating recovery and enabling complementary functionalities (e.g., metal chelation and antibacterial action) essential for efficient water purification.

Results and discussion

Porous chitosan versus alginate beads

Porous chitosan microspheres were first prepared by coagulating an acidic chitosan solution in a basic bath, as shown in Fig. 1 (see the Experimental section for details).[18] For comparison, porous calcium cross-linked alginate beads were also prepared for the same purpose (Fig. S1, SI). For clarity, beads immersed in water and not subjected to drying are denoted as CS_HB and Alg_HB, where HB stands for hydrogel beads. Xerogel beads air-dried under ambient conditions are denoted as XB, while freeze-dried beads are referred to as CB (cryogel beads). Because both chitosan and alginate are low-cost, readily form self-standing porous beads, and can be post-functionalized, our preliminary screening aimed to identify the most suitable bead-forming biopolymer. Comparative adsorption tests using syringic acid were conducted on both bead types (Fig. S2, SI). After 120 min of contact, chitosan and calcium–alginate beads achieved 26% and 20% uptake, respectively. Although the performance difference was modest, chitosan beads exhibited higher reproducibility, stability over time, and structural integrity, whereas alginate beads showed fluctuations in syringic acid retention and deformation of their spherical shape (Fig. S3a, SI). We therefore pursued further work with chemically and texturally engineered chitosan beads. Fig. S3b illustrates their appearance before and after syringic acid adsorption, showing no visible change in shape. DRIFT spectra of chitosan before and after adsorption revealed no significant variation (Fig. S4, SI), confirming the physical stability of the matrix.

Screening different fillers entrapping porous chitosan beads

Considering the moderate uptake achieved by unmodified chitosan hydrogel beads, we next incorporated a second phase to enhance adsorption performance. As previously discussed, chitosan can be readily hybridized via electrostatic interactions during gelation.[18,20] Accordingly, we embedded various fillers within chitosan hydrogels and evaluated their performance in olive mill wastewater (OMW) treatment. Different filler-containing chitosan beads were synthesized using sepiolite (SEP), halloysite (HNT), and montmorillonite (MMT) as representative clays; activated carbon (AC) and reduced graphene oxide (rGO) as carbonaceous materials; and carbon nitride (C_3N_4) as nitrogen-rich graphitic sheets. Each filler was dispersed into the aqueous acidic chitosan solution, followed by vigorous magnetic stirring for 2 h before coagulation in NaOH solution, where chitosan precipitates upon deprotonation of amino groups (see the Experimental section). Droplet-wise introduction of chitosan into the basic bath preserved their spherical shape, yielding self-standing microspheres. This pH-induced gelation forms a secondary structure in which polysaccharide fibers entangle into a three-dimensional network, while the fillers are anchored via hydrogen bonding and electrostatic interactions. Literature reports indicate that each hydrogel bead typically contains 2–3 wt% of solid matter dispersed in 97–98 wt% water,[20] reflecting their high open porosity (Fig. 2). Herein, we have selected a CS:filler ratio of 90 : 10, although other ratios can be employed without impairing the bead-forming ability of chitosan.[18]

Digital images confirmed the successful formation of self-standing composite beads (Fig. 2). Activated carbon and rGO-loaded beads (CS@AC_90:10_HB and CS@rGO_90:10_HB) were easily identifiable by their black coloration (Fig. 2d and e).
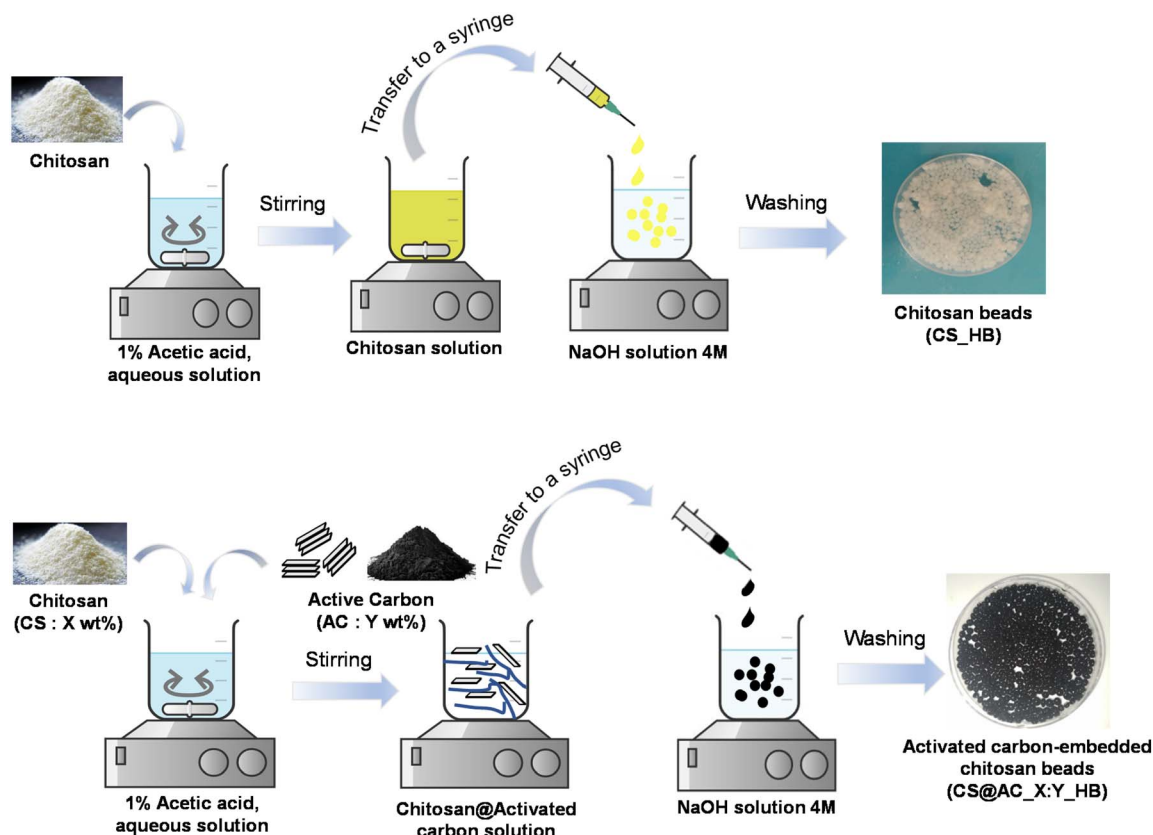
Fig. 1 Multistep preparation of porous chitosan hydrogel beads (CS_HB) and activated carbon-containing chitosan beads (CS@AC_X:Y_HB) with X and Y referring to the weight percentage of chitosan and activated carbon, respectively.
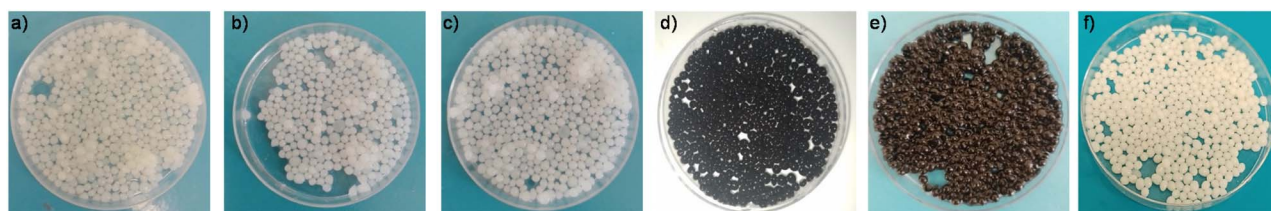

Fig. 2 Chitosan beads entrapping different fillers: (a) CS@MMT_90:10_HB, (b) CS@HNT_90:10_HB, (c) CS@SEP_90:10_HB, (d) CS@AC_90:10_HB, (e) CS@rGO_90:10_HB, and (f) CS@C$_3$N$_4$_90:10_HB.

The adsorption performance of these hydrogel beads toward syringic acid is shown in Fig. S5a (SI). Pristine chitosan hydrogels exhibited moderate adsorption (33% after 24 h), whereas filler-modified beads showed substantial improvement, with CS@AC_90:10_HB achieving the highest uptake of 54% (Fig. S5b, SI). Among the clay-filled systems, montmorillonite (MMT) performed best, confirming its beneficial incorporation within the chitosan beads.

Porous chitosan@activated carbon *versus* chitosan@MMT beads

Based on these results, MMT and AC were selected for further characterization and investigation. This choice was motivated by their abundance, proven adsorption performance, and contrasting structural behaviours (exfoliation, intercalation, or agglomeration) depending on the polymer-to-filler ratio (Fig. S6, SI).[34,39]

We prepared chitosan beads containing 50 wt% of either activated carbon (CS@AC_50:50) or montmorillonite (CS@MMT_50:50). The hydrogel precursors (CS@AC_50:50_HB and CS@MMT_50:50_HB) were porous, and their behaviour during drying reflected both water affinity and mechanical stability of the network imparted by the filler.

SEM analysis of the corresponding freeze-dried beads (CS@AC_50:50_CB and CS@MMT_50:50_CB) was compared with that of pristine components (Fig. 3). Activated carbon consisted of agglomerated, porous, interconnected particles, while MMT exhibited stacked, flake-like aggregates (Fig. S7, SI). Pristine chitosan beads showed a dense, smooth, nonporous surface, typical of collapsed polysaccharides (Fig. 3, left). Cross-
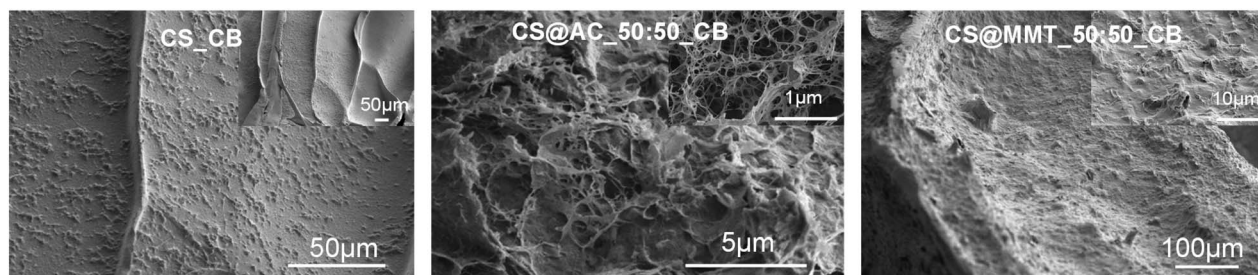
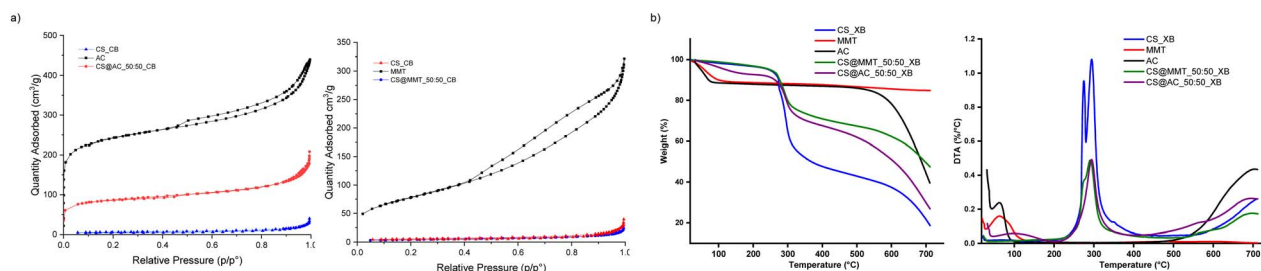**Fig. 3** SEM analysis of CS_CB, CS@AC_50:50_CB and CS@MMT_50:50_CB.

Fig. 4 Textural and thermal properties of modified beads and their individual components. (a) Nitrogen sorption analysis of CS@AC_50:50_CB versus CS@MMT_50:50_CB beads. (b) Thermogravimetric analysis of CS@AC_50:50_XB versus CS@MMT_50:50_XB beads plotted against pristine CS_XB, AC and MMT.

sections of CS@MMT_50:50_CB beads revealed a compact, smooth network similar to pristine chitosan, suggesting that clay particles were embedded within collapsed polymer chains (Fig. 3, right). In contrast, CS@AC_50:50_CB beads displayed a well-entangled nanofibrous texture with numerous voids, indicating a significantly porous framework (Fig. 3, middle). The activated carbon particles appeared well dispersed and interacted with polysaccharide fibers through edge functionalities, introducing surface roughness and hierarchical porosity.

Nitrogen physisorption confirmed these observations. Pristine AC and MMT exhibited surface areas of 764 m^2 g^{-1} and 282 m^2 g^{-1}, respectively (Fig. 4a and Table S1). Air-dried chitosan beads (CS_XB) displayed negligible porosity, as polysaccharide chains collapsed upon water removal.[40,41] A sharp contrast was observed between CS@AC_50:50_XB (141 m^2 g^{-1}) and CS@MMT_50:50_XB (2 m^2 g^{-1}). The high hydrophilicity of MMT induces strong water-solid interactions and capillary forces during drying, leading to network collapse. Conversely, the hydrophobic nature of AC minimizes water binding and preserves pore structure.

Freeze-drying greatly enhanced porosity, yielding surface areas of 310 m^2 g^{-1} for CS@AC_50:50_CB and 16 m^2 g^{-1} for CS@MMT_50:50_CB (Fig. 4). The porosity of CS@AC_50:50_CB is approximately half that of native AC, consistent with shrinkage of the polymer matrix and the macroporosity introduced by ice-templating. These results highlight the opposite behaviours of the two fillers, where AC enhances porosity, while MMT reinforces structural stability.

Thermogravimetric analysis (TGA/DTA) further confirmed these trends. Pristine chitosan degraded in two main steps:

a ∼50% mass loss between 250 and 400 °C (deacetylation and glycosidic bond cleavage) followed by gradual oxidation above 400 °C. Activated carbon showed minimal weight loss (<10%) below 150 °C due to moisture removal, remaining stable up to ∼550 °C. Montmorillonite exhibited only ∼10% total mass loss, attributed to interlayer water removal. Composite beads displayed enhanced stability: the degradation onset shifted from 307 °C for pristine chitosan to 524 °C for CS@AC_50:50_XB and 630 °C for CS@MMT_50:50_XB. The increased residual mass and delayed decomposition confirm polymer reinforcement by both fillers, with MMT providing the most pronounced thermal protection (Fig. 4b and Table S2). The residue at 700 °C matched the theoretical 50 : 50 composition ratio, confirming accurate filler incorporation and homogeneous dispersion. In summary, activated carbon contributes primarily to porosity development, while montmorillonite enhances thermal and mechanical stability.

We next examined how the chitosan-to-filler weight ratio influences the uptake of syringic acid and caffeic acid, used as representative polyphenolic pollutants (Fig. 5). For syringic acid, adsorption performance increased proportionally with the amount of activated carbon incorporated within the hydrogels, with the CS@AC_50:50_HB composition showing the highest efficiency, achieving an impressive 99% removal after 24 hours (Fig. 5a). In contrast, hydrogel beads loaded with montmorillonite (MMT) exhibited inferior performance compared to those containing activated carbon. The optimal formulation among these beads was CS@MMT_90:10_HB, which reached a maximum removal rate of 45% after 24 hours (Fig. 5a).
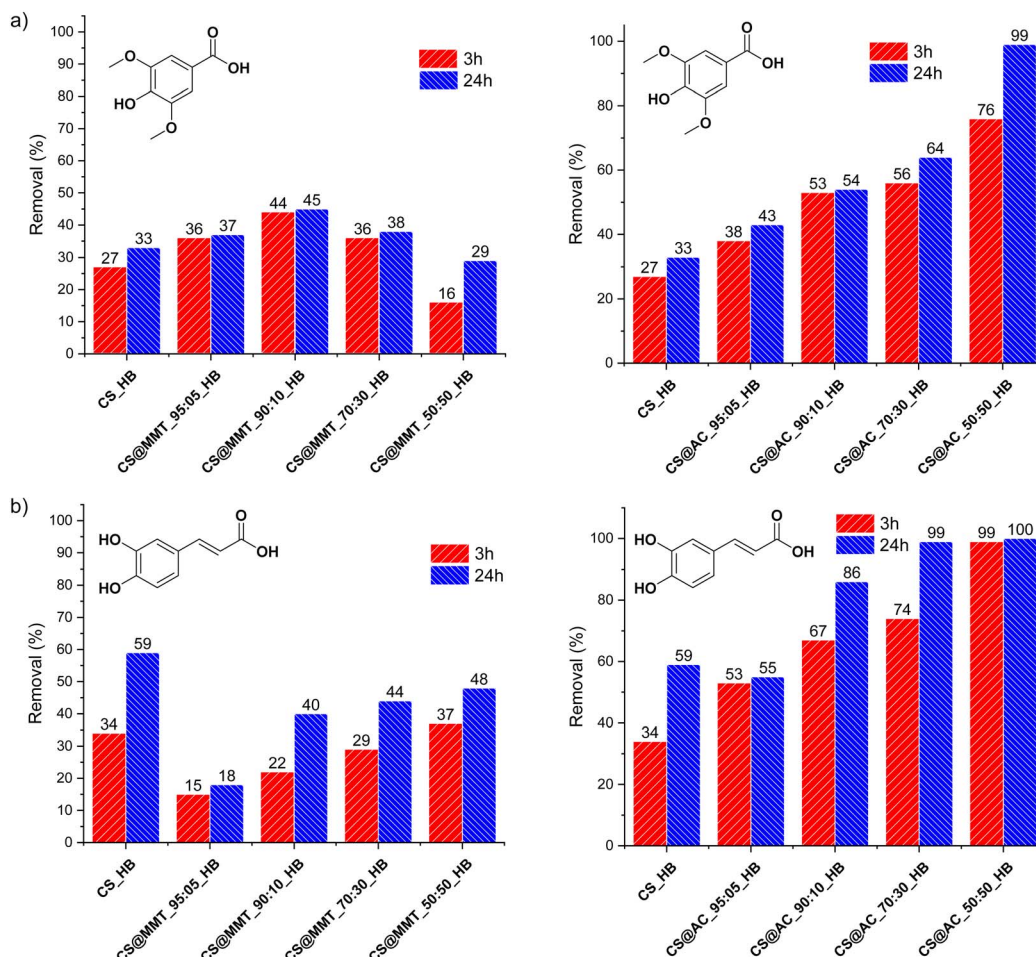
Fig. 5 Effect of the filler loading on (a) the syringic acid uptake and (b) the caffeic acid uptake using chitosan entrapping montmorillonite CS@MMT_*X:Y*_HB and chitosan entrapping activated carbon CS@AC_*X:Y*_HB.

Similarly, CS@AC_HB nanocomposite beads demonstrated the best performance toward caffeic acid, achieving removal rates of 86%, 99%, and 100% for CS@AC_90:10_HB, CS@AC_70:30_HB, and CS@AC_50:50_HB, respectively. These values far exceeded those of the corresponding CS@MMT_HB samples (Fig. 6b). Interestingly, MMT-containing beads were even less efficient than pristine chitosan hydrogels, suggesting that montmorillonite exhibits little affinity for caffeic acid. The observed decline in adsorption efficiency with increasing MMT content likely arises from the agglomeration of MMT into microparticles, tactoids, and less-reactive aggregates, which may also obstruct the hydrogel pores.[42]

As previously mentioned, the adsorption performance of CS@AC_HB correlates positively with the amount of activated carbon, highlighting its strong affinity for polyphenolic contaminants. Visual inspection of the beads before and after adsorption revealed noticeable color changes in CS@MMT_HB following caffeic acid adsorption, whereas no color change was observed after syringic acid treatment (Fig. S8, SI). In both cases, the beads retained their shape, sphericity, and structural integrity, indicating that they can be easily recovered from water and potentially reused (Fig. S9, SI).

To further demonstrate the advantages of open-porous hydrogels, analogous xerogel beads obtained by air drying were tested. These xerogels exhibited reduced porosity compared to their native hydrogel counterparts. When exposed to syringic acid and caffeic acid solutions ($C = 10^{-4}$ mmol g^{-1}), the CS@AC_50:50_XB xerogel beads achieved only 60% and 62% uptake after three hours, respectively, compared to 76% and 99% for the corresponding hydrogels (Fig. 6a and b). This result clearly underscores the importance of an open porous framework for efficient adsorption.

Additional differences between hydrogels and xerogels emerged during recyclability tests, which stand as an essential attribute of shaped chitosan materials.[30] The self-standing hydrogel beads could be conveniently removed from the reaction medium using a spatula, eliminating the need for any workup steps such as filtration or centrifugation.[24] This practicality translated into excellent reusability: CS@AC_50:50_HB maintained removal efficiencies of 66% and 94% for syringic acid and caffeic acid, respectively, after four adsorption–desorption cycles. In contrast, the xerogel analogues showed a severe decline in performance, with removal rates dropping to
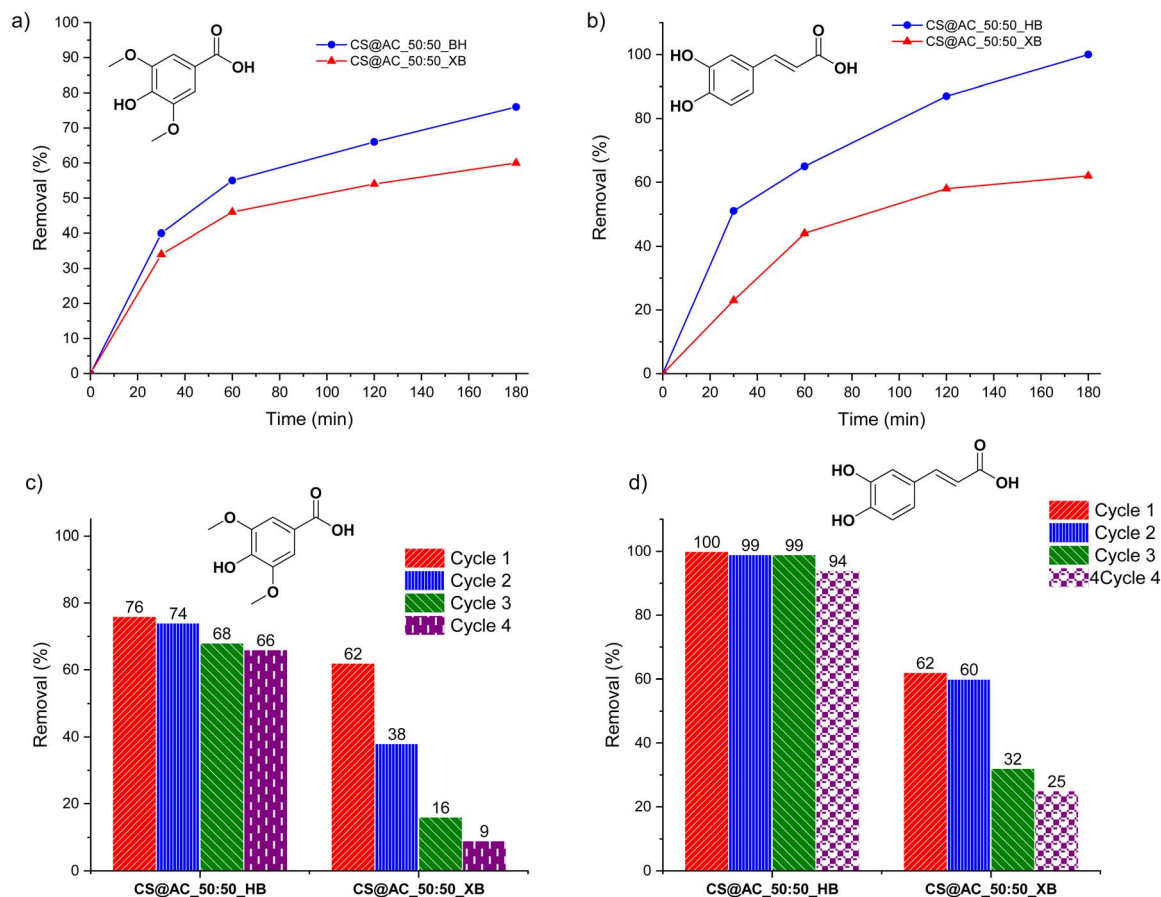
Fig. 6 Adsorption kinetics and recycling performance of hydrogel and xerogel beads on syringic acid and caffeic acid: (a) kinetics of syringic acid adsorption, (b) kinetics of caffeic acid adsorption, (c) recycling performance for syringic acid, and (d) recycling performance for caffeic acid.

9% and 25% for syringic acid and caffeic acid, respectively, after four cycles (Fig. 6c and d).

Treatment of real OMW over porous chitosan-filled beads

Finally, AC- and MMT-containing chitosan hydrogel beads were tested for direct OMW treatment under batch conditions. The raw OMW was diluted to avoid site saturation, reduce acidity, and maintain bead integrity. Characteristics of raw, diluted, and treated OMW are summarized in Table S3a. As expected, CS@AC_50:50_HB was the most efficient adsorbent, removing

95% of OMW within 24 h. CS@MMT_50:50_HB achieved 69% removal, which is acceptable but significantly lower (Fig. 7). While AC-containing beads showed a clear dependence of adsorption capacity on AC loading, MMT-based systems exhibited more complex behavior involving layered-clay transformations (tactoid, intercalated, and exfoliated) and dynamic chitosan intercalation,[39,42–45] complicating optimization. In addition to its open porous structure and hydrophobic character, activated carbon offers diverse adsorption sites, including oxygenated edge groups and basal planes capable of π–π stacking with aromatic polyphenols.[46]
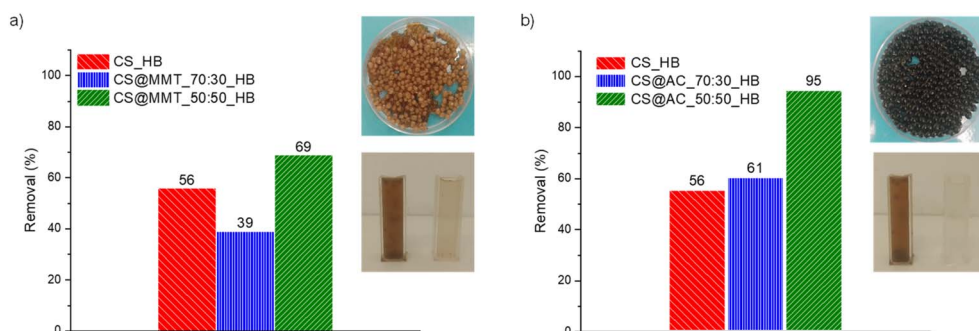

Fig. 7 Olive mill wastewater treatment using (a) chitosan entrapping montmorillonite CS@MMT_HB and (b) chitosan entrapping activated carbon CS@AC_HB.

Photographic evidence (Fig. 7) shows that treated OMW solutions became nearly transparent after adsorption with CS@AC_50:50_HB. Quantitatively, this system achieved remarkable reductions: 78% COD, 93% BOD_5, 100% turbidity, 79% conductivity, 85% salinity, and overall 95% total OMW removal (Table S3b, SI). The synergistic effect between chitosan and activated carbon likely accounts for this outstanding performance.

Beyond wastewater purification, these polyphenol-enriched chitosan beads could be valorized in agriculture, fertilizers, food preservation, or as functional adsorbents. As a proof of concept, OMW-saturated beads (CS_HB_OMW, CS@MMT_50:50_HB_OMW, and CS@AC_50:50_HB_OMW) were tested for secondary adsorption of model pollutants, namely, Congo Red (CR), Cu^{2+} ions, and tetracycline (TC) (Fig. S10, SI). Remarkably, the presence of OMW residues did not hinder further adsorption. CS@AC_50:50_HB_OMW removed 99% of CR, 86% of TC, and 44% of Cu^{2+}, confirming its multifunctionality. These preliminary results demonstrate the feasibility of using OMW-enriched microspheres as precursors for extended pollutant remediation, paving the way toward circular, waste-to-resource processing of olive mill effluents.

Experimental

Starting reagents

All commercially available reagents and solvents were used without additional purification. Chitosan of medium molecular weight (viscosity: 200–800 cps, degree of deacetylation $\approx 80\%$) was purchased from Sigma-Aldrich (CAS No. 9012-76-4). Sodium alginate (CAS No. 9005-38-3, product reference 27660.296) was supplied by VWR Chemicals. Caffeic acid ($\geq 98\%$, CAS 331-39-5) and syringic acid ($\geq 98\%$, CAS 530-57-4) were obtained from Alfa Aesar. Copper(II) nitrate trihydrate $[Cu(NO_3)_2 \cdot 3H_2O]$ was provided by Solvachim, and calcium chloride ($CaCl_2$, CAS 10035-04-8) by Sigma-Aldrich. Natural montmorillonite (MMT) was acquired from Southern Clay Products Inc. (Gonzales, Texas) under the trade name Cloisite-Na^+. It was supplied as a fine powder with a cation exchange capacity (CEC) of 95 meq/100 g and an interlayer spacing (d_{001}) of 1.2 nm. Sepiolite (SEP) was supplied by TOLSA with a purity above 85%, consisting of slightly aggregated fibers several micrometers long. Halloysite nanotubes (HNTs) were obtained from Dragonite, with the following characteristics: length = 0.2–2 µm, outer diameter = 50–70 nm, and inner diameter = 15–45 nm. Activated carbon (AC) was purchased from Sigma-Aldrich (CAS 7440-44-0). Reduced graphene oxide (rGO) was synthesized following a previously reported procedure.[47] Graphitic carbon nitride (g-C_3N_4) was prepared *via* a two-step thermal polymerization of urea.[48] Urea was first calcined in a covered crucible in air at 550 °C for 4 h (heating rate: 2.5 °C min^{-1}). The resulting yellowish powder was then placed in an open crucible and thermally treated at 500 °C for 2 h to complete condensation. The obtained material was washed thoroughly with distilled water to remove residual alkaline species and dried at 60 °C overnight. Olive mill wastewater (OMW) samples were collected from a semi-traditional three-phase olive oil extraction unit located in the rural commune of Laajajra, Moulay Yaâcoub Province, Fez-Boulemane region (Morocco). The OMW samples were first characterized, then stored in sealed bottles at 4 °C in the dark until use.

Materials characterization

Comprehensive physicochemical characterization of the adsorbent materials was conducted to evaluate their structural, thermal, and surface properties before and after exposure to OMW. Fourier-transform infrared (FTIR) spectra were recorded using a Perkin-Elmer Spectrum 100 spectrometer equipped with an ATR accessory. Spectra were collected in the 4000–600 cm^{-1} range at a resolution of 4 cm^{-1}, averaging 32 scans. Thermogravimetric analysis (TGA) was carried out on a TA Instruments Q500 analyzer under air, from ambient temperature to 750 °C, at a heating rate of 20 °C min^{-1}. Hydrogel microspheres were dried at 80 °C for 24 h prior to analysis to ensure accurate thermal behavior evaluation. Nitrogen adsorption–desorption isotherms were measured at 77 K using a Micromeritics Tristar II Plus analyzer. Samples were degassed at 100 °C for 48 h before analysis. The specific surface area (S_{BET}) was determined by the multipoint BET method in the relative pressure range 0.04–0.25. The total pore volume was estimated from the amount of nitrogen adsorbed at $P/P_0 = 0.99$. Scanning electron microscopy (SEM) images were obtained using a JEOL JSM-6700F microscope. UV-visible absorbance spectra were recorded in the 200–800 nm range on a PerkinElmer Lambda 1050 spectrophotometer.

OMW characterization

Basic physicochemical parameters of raw and treated OMW were analyzed. pH was measured using a JENCO pH meter, while turbidity was determined with an ISO-certified turbidimeter (HI 88713, HANNA Instruments). Electrical conductivity, total dissolved solids (TDS), and salinity were measured using a multiparameter conductometer (inoLab – WTW). Chemical oxygen demand (COD) and biochemical oxygen demand (BOD_5) were used to assess the oxidative potential and biodegradability of the wastewater. COD was determined by the standard closed reflux method using an ISCO RECOD reactor, involving acidic oxidation with potassium dichromate followed by UV-vis analysis at 600 nm. BOD_5 was measured using a manometric OxiTop IS 6 – WTW system after five days of incubation at 20 °C.

Preparation of chitosan-based hydrogel beads

A viscous chitosan solution was prepared by dissolving 1.0 g of chitosan in 50 mL of 1% (v/v) acetic acid under vigorous magnetic stirring for 3 h at room temperature. The resulting solution was dropped into a 4 M NaOH coagulation bath using a syringe fitted with a 0.8 mm needle, producing spherical hydrogel beads. The beads were kept in the alkaline medium for 3 h to ensure complete gelation, then collected by filtration and rinsed thoroughly with distilled water until a neutral pH was achieved. Native chitosan hydrogel beads are denoted as CS_HB.

Preparation of composite hydrogel beads entrapping nanometric fillers

To prepare reinforced composites, a fixed chitosan-to-filler mass ratio of 90:10 was used (900 mg chitosan + 100 mg filler). Reinforcing agents included carbon-based additives (AC, rGO, and g-C$_3$N$_4$) and mineral phases (MMT, SEP, and HNT). Each filler was homogeneously dispersed in the chitosan solution before bead formation, following the same gelation protocol as the native beads. The resulting composites were labeled CS@AC_90:10_HB, CS@rGO_90:10_HB, CS@C$_3$-N$_4$_90:10_HB, CS@MMT_90:10_HB, CS@SEP_90:10_HB, and CS@HNT_90:10_HB.

Optimized composite systems and ratio variation

Among the tested composites, CS@AC_90:10_HB and CS@MMT_90:10_HB exhibited the most promising adsorption performance and were selected for optimization. To study the effect of filler content, additional formulations were prepared with chitosan-to-filler ratios of 70:30 and 50:50, designated as CS@AC_70:30_HB, CS@MMT_70:30_HB, CS@AC_50:50_HB, and CS@MMT_50:50_HB, following the same synthesis procedure.

Preparation of chitosan and composite cryogel beads

The hydrogel beads were rapidly frozen by immersion in liquid nitrogen (without direct contact) to prevent large ice crystal formation and preserve the internal porosity and surface area. The frozen beads were then freeze-dried under vacuum at −50 °C. The resulting cryogel beads were labeled CS_CB for native chitosan, CS@AC_50:50_CB for chitosan-activated carbon, and CS@MMT_50:50_CB for chitosan–montmorillonite composites.

Preparation of chitosan and composite-based xerogel beads

Xerogel beads were obtained by drying the hydrogel beads in an oven at 80 °C for 24 h. The dried materials were denoted using the suffix "_XB", such as CS_XB for native chitosan and CS@AC_50:50_XB for chitosan–activated carbon composites.

Polyphenols batch adsorption tests

Adsorption experiments were performed by contacting the prepared adsorbents with caffeic acid or syringic acid solutions (initial concentration = 10^{-4} mol L^{-1}). The solid-to-liquid ratio was 1:1 (w/v), corresponding to 1 mg of hydrogel beads per 1 mL of solution. At predetermined time intervals, aliquots were withdrawn, and UV-vis absorbance was measured at 267 nm (syringic acid) and 316 nm (caffeic acid).

The removal efficiency (% R) was calculated as:

$$\% \text{ Removal} = \frac{C_i - C_t}{C_i} \times 100$$

where C_i and C_t are the initial and time-dependent concentrations, respectively.

OMW batch adsorption tests

OMW adsorption tests were carried out under the same conditions as the polyphenol experiments. The OMW stock solution was diluted 1:100 with distilled water before use. Adsorption progress was monitored by UV-vis absorbance at 280 nm.

Congo red, tetracycline and copper nitrate batch adsorption tests

To evaluate the residual adsorption capacity of the beads after OMW treatment, additional tests were conducted using model pollutants (Congo red, tetracycline, and copper nitrate), each at an initial concentration of 10^{-4} mol L^{-1} and an adsorbent-to-solution ratio of 1:1 (w/v). UV-vis absorbance was measured at 498 nm (Congo red), 356 nm (tetracycline), and 780 nm (copper nitrate).

Regeneration and reuse of the beads

Reusability was evaluated through successive adsorption–desorption cycles under identical experimental conditions using syringic and caffeic acids as model polyphenols. After each adsorption cycle, beads were regenerated by washing thoroughly with distilled water (three to four rinses over 3 h under vigorous agitation) to desorb retained compounds before reuse.

Treatment efficiency assessment

The overall treatment efficiency was evaluated using the percentage removal (% R) of various pollutants, including dissolved organic molecules (caffeic acid and syringic acid), copper nitrate, tetracycline, and key OMW physicochemical parameters (UV-vis absorbance, COD, BOD$_5$, TDS, etc.), calculated as:

$$\% \text{ Removal} = \frac{C_i - C_t}{C_i} \times 100$$

where C_i and C_t represent the initial and final parameter values, respectively.

Conclusions

In summary, we report a proof of concept demonstrating the use of chitosan beads as recyclable reactors for the treatment of olive mill wastewater. We show that efficient adsorbents can be engineered by combining chitosan biopolymer with activated carbon, and to a lesser extent, montmorillonite clay particulates. A contrasting behavior was observed depending on the type of filler: activated carbon proved more effective in opening the chitosan network, while montmorillonite contributed to enhancing thermal stability. The adsorptive performance of activated carbon-containing beads increased with filler loading, underscoring its key role in scavenging polyphenolic compounds. In contrast, the montmorillonite-based beads displayed more moderate performance, likely due to dynamic factors such as clay delamination and the ingress–egress behavior of chitosan chains within the interlayer galleries.

Importantly, the beads can be readily recovered from the medium and recycled multiple times without requiring tedious workup procedures. Their successful application to the treatment of mixed effluents further validates their versatility and highlights their potential for advancing circular economy principles in wastewater management.

Conflicts of interest

There are no conflicts to declare.

Data availability

The data supporting this article have been included as part of the supplementary information (SI). Supplementary information: various information related to the experimental protocols, DRIFT spectra, SEM and nitrogen physisorption. See DOI: https://doi.org/10.1039/d5su00592b.

Acknowledgements

Notes and references

1 S. Shabir, N. Ilyas, M. Saeed, F. Bibi, R. Z. Sayyed and W. H. Almalki, *Environ. Res.*, 2023, **216**, 114399.

2 A. Roig, M. L. Cayuela and M. A. Sánchez-Monedero, *Waste Manag.*, 2006, **26**, 960–969.

3 E. P. Kalogianni, D. Georgiou and J. H. Hasanov, *J. Am. Oil Chem. Soc.*, 2019, **96**, 481–507.

4 S. Dermeche, M. Nadour, C. Larroche, F. Moulti-Mati and P. Michaud, *Process Biochem.*, 2013, **48**, 1532–1552.

5 P. Paraskeva and E. Diamadopoulos, *J. Chem. Technol. Biotechnol.*, 2006, **81**, 1475–1485.

6 Z. S. Lee, S. Y. Chin, J. W. Lim, T. Witoon and C. K. Cheng, *Environ. Technol. Innovation*, 2019, **15**, 100377.

7 M. R. Zahi, W. Zam and M. El Hattab, *Food Chem.*, 2022, **381**, 132238.

8 A. Jamrah, T. M. Al-Zghoul and M. M. Darwish, *Chem. Environ. Eng.*, 2023, **8**, 100493.

9 N. Solomakou and A. M. Goula, *Rev. Environ. Sci. Biotechnol.*, 2021, **20**, 839–863.

10 N. El Messaoudi, M. El Khomri, A. El Mouden, A. Bouich, A. Jada, A. Lacherai, H. M. N. Iqbal, S. I. Mulla, V. Kumar and J. H. P. Américo-Pinheiro, *Biomass Convers. Biorefin.*, 2024, **14**, 11739–11756.

11 R. Rashid, I. Shafiq, P. Akhter, M. J. Iqbal and M. Hussain, *Environ. Sci. Pollut. Res.*, 2021, **28**, 9050–9066.

12 A. I. Osman, E. M. A. El-Monaem, A. M. Elgarahy, C. O. Aniagor, M. Hosny, M. Farghali, E. Rashad, M. I. Ejimofor, E. A. López-Maldonado, I. Ihara, P.-S. Yap, D. W. Rooney and A. S. Eltaweil, *Environ. Chem. Lett.*, 2023, **21**, 2337–2398.

13 A. M. Salaberria, J. Labidi and S. C. M. Fernandes, *Eur. Polym. J.*, 2015, **68**, 503–515.

14 N. Yan and X. Chen, *Nature*, 2015, **524**, 155–157.

15 A. El Kadib, *ChemSusChem*, 2015, **8**, 217–244.

16 F. J. Pavinatto, L. Caseli and O. N. Oliveira, *Biomacromolecules*, 2010, **11**, 1897–1908.

17 I. Junceda-Mena, E. García-Junceda and J. Revuelta, *Carbohydr. Polym.*, 2023, **309**, 120674.

18 A. El Kadib, *Chem. Rec.*, 2020, **20**, 753–772.

19 A. El Kadib, M. Bousmina and D. Brunel, *J. Nanosci. Nanotechnol.*, 2014, **14**, 308–331.

20 A. El Kadib and M. Bousmina, *Chem.–Eur. J.*, 2012, **18**, 8264–8277.

21 B. Boumhidi, N. Katir, J. El Haskouri, K. Draoui and A. El Kadib, *New J. Chem.*, 2020, **44**, 14136–14144.

22 N. Hammi, M. Bonneau, A. El Kadib, S. Kitagawa, T. Loiseau, C. Volkringer, S. Royer and J. Dhainaut, *ACS Appl. Mater. Interfaces*, 2023, **15**, 53395–53404.

23 N. Hammi, N. Couzon, T. Loiseau, C. Volkringer, A. El Kadib, S. Royer and J. Dhainaut, *Mater. Today Sustain.*, 2023, **22**, 100394.

24 S. Frindy, A. Primo, M. Lahcini, M. Bousmina, H. Garcia and A. El Kadib, *Green Chem.*, 2015, **17**, 1893–1898.

25 S. Frindy, A. El Kadib, M. Lahcini, A. Primo and H. García, *ChemCatChem*, 2015, **7**, 3307–3315.

26 N. Hammi, S. Chen, A. Primo, S. Royer, H. Garcia and A. El Kadib, *Green Chem.*, 2022, **24**, 4533–4543.

27 F.-E. Zirar, N. Katir, S. Qourzal, I. A. Ichou and A. El Kadib, *RSC Adv.*, 2022, **12**, 21145–21152.

28 S. Frindy, A. Primo, H. Ennajih, A. el kacem Qaiss, R. Bouhfid, M. Lahcini, E. M. Essassi, H. Garcia and A. El Kadib, *Carbohydr. Polym.*, 2017, **167**, 297–305.

29 N. Hammi, M. Kędzierska, N. Wrońska, N. Katir, J. Dhainaut, S. Royer, K. Lisowska, M. Bryszewska, K. Miłowska and A. El Kadib, *Mater. Adv.*, 2023, **4**, 5191–5199.

30 S. Takeshita, S. Zhao, W. J. Malfait and M. M. Koebel, *Angew. Chem., Int. Ed.*, 2021, **60**, 9828–9851.

31 S. A. Khan and T. A. Khan, *J. Environ. Chem. Eng.*, 2021, **9**, 105575.

32 M. M. Sabzehmeidani, S. Mahnaee, M. Ghaedi, H. Heidari and V. A. L. Roy, *Mater. Adv.*, 2021, **2**, 598–627.

33 A. E. Burakov, E. V. Galunin, I. V. Burakova, A. E. Kucherova, S. Agarwal, A. G. Tkachev and V. K. Gupta, *Ecotoxicol. Environ. Saf.*, 2018, **148**, 702–712.

34 I. Pet, M. N. Sanad, M. Farouz, M. M. ElFaham, A. El-Hussein, M. S. A. El-sadek, R. A. Althobiti and A. Ioanid, *Water Conserv. Sci. Eng.*, 2024, **9**, 62.

35 J. P. Gutkoski, E. E. Schneider and C. Michels, *J. Environ. Manage.*, 2024, **349**, 119434.

36 A. K. Thakur, R. Singh, R. Teja Pullela and V. Pundir, *Mater. Today: Proc.*, 2022, **57**, 1468–1472.

37 J. He, Q. Zhou, J. Guo, J. Gao and F. Fang, *J. Hazard. Mater.*, 2020, **384**, 121501.

38 L. Wang and N. Balasubramanian, *Chem.–Eng. J.*, 2009, **155**, 763–768.

39 M. Bousmina, *Macromolecules*, 2006, **39**, 4259–4263.

40 R. Valentin, K. Molvinger, F. Quignard and D. Brunel, *New J. Chem.*, 2003, **27**, 1690–1692.

41 F. Quignard, R. Valentin and F. Di Renzo, *New J. Chem.*, 2008, **32**, 1300–1310.

42 H. Ennajih, R. Bouhfid, E. M. Essassi, M. Bousmina and A. El Kadib, *Microporous Mesoporous Mater.*, 2012, **152**, 208–213.

43 E. Ruiz-Hitzky, C. Ruiz-Garcia and X. Wang, *Chem. Mater.*, 2023, **35**, 10295–10315.

44 P. Aranda and E. Ruiz-Hitzky, *Chem. Mater.*, 1992, **4**, 1395–1403.

45 M. Darder, M. Colilla and E. Ruiz-Hitzky, *Chem. Mater.*, 2003, **15**, 3774–3780.

46 M. Gayathiri, T. Pulingam, K. T. Lee and K. Sudesh, *Chemosphere*, 2022, **294**, 133764.

47 S. N. Alam, N. Sharma and L. J. G. Kumar, *Graphene*, 2017, **6**, 1.

48 A. Amedlous, M. Majdoub, E. Amaterz, Z. Anfar and A. Benlhachemi, *J. Photochem. Photobiol., A*, 2021, **409**, 113127.